Biophysical Chemistry 184 (2013) 54–61

Contents lists available at ScienceDirect

Biophysical Chemistry

journal homepage: http://www.elsevier.com/locate/biophyschem

Epitaxial assembly dynamics of mutant amyloid β25–35_N27C fibrils explored with time-resolved scanning force microscopy

Miklós S.Z. Kellermayer [a,*], Ünige Murvai [a], Andrea Horváth [a], Emőke Lászlóffi [a], Katalin Soós [b], Botond Penke [c]

[a] Department of Biophysics and Radiation Biology, Semmelweis University, Tűzoltó u. 37-47, Budapest H1094, Hungary
[b] Department of Medical Chemistry, University of Szeged, Dóm tér 8., Szeged H-6720, Hungary
[c] Supramolecular and Nanostructured Materials Research Group of the Hungarian Academy of Sciences, Dóm tér 8., Szeged H-6720, Hungary

HIGHLIGHTS

- Epitaxial assembly kinetics of mutant amyloid β25–35_N27C fibrils on mica were investigated.
- Fibril growth kinetics were followed as a function of peptide and KCl concentrations.
- Critical peptide concentration for fibril assembly was 3.92 μM, maximum growth rate 0.38 nm/s.
- Above 20 mM KCl mutant fibril growth stopped even at high peptide concentrations.
- With peptide and KCl concentrations the structure of Aβ25–35_N27C fibril nano-network can be tuned.

GRAPHICAL ABSTRACT

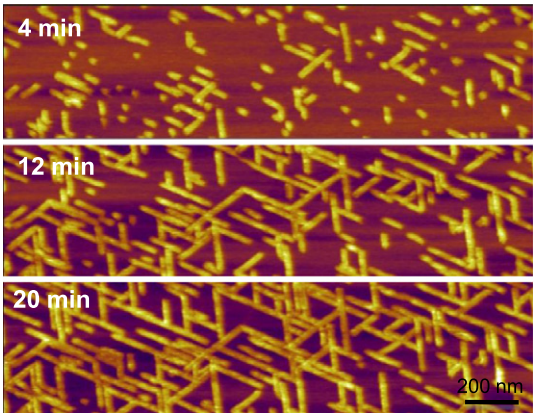

ARTICLE INFO

Article history:
Received 21 July 2013
Received in revised form 28 August 2013
Accepted 28 August 2013
Available online 5 September 2013

Keywords:
Amyloid
Atomic force microscopy
Epitaxial growth
Nanoscale network
Sulfhydryl chemistry
Scanning force kymography

ABSTRACT

Amyloid β25–35 (Aβ25–35) is a toxic fragment of Alzheimer's beta peptide. We have previously shown that Aβ25–35 fibrils form a trigonally oriented network on mica by epitaxial growth mechanisms. Chemical reactivity can be furnished to the fibril by introducing a cysteine residue (Aβ25–35_N27C) while maintaining oriented assembly properties. Previously we have shown that fibril binding to mica is strongly influenced by KCl concentration. In the present work we explored the kinetics of epitaxial assembly of the mutant fibrils at different peptide and KCl concentrations by using in situ time-resolved AFM. We measured the length of Aβ25–35_N27C fibrils as a function of time. Increasing free peptide concentration enhanced fibril growth rate, and the critical peptide concentration of fibril assembly was 3.92 μM. Increasing KCl concentration decreased the number of fibrils bound to the mica surface, and above 20 mM KCl fibril formation was completely abolished even at high peptide concentrations. By modulating peptide and KCl concentrations in the optimal ranges established here the complexity of the Aβ25–35_N27C network can be finely tuned.

1. Introduction

Amyloid fibrils are proteinaceous filaments which, under *in vivo* conditions and in a variety of degenerative diseases, become deposited in the extracellular space of different tissues [1–4]. Amyloid fibrils have been shown to function as nanoscale templates for electrically

* Corresponding author. Tel.: +36 20 825 9994; fax: +36 1 266 6656.
E-mail address: kellermayer.miklos@med.semmelweis-univ.hu (M.S.Z. Kellermayer).

0301-4622/$ – see front matter © 2013 Elsevier B.V. All rights reserved.
http://dx.doi.org/10.1016/j.bpc.2013.08.007

conductive nanowires, raising the possibility of their nanotechnological applications. A genetically engineered segment of the *Saccharomyces cerevisiae* Sup35p protein was used as a template for the deposition of colloidal gold and metallic silver, thereby generating nanoscale wires with ohmic properties [5]. The Alzheimer β-amyloid diphenylalanine structural motif was used to generate nanotubes within which metallic silver was deposited, forming long metallic nanowires [6]. The self-assembly properties of amyloidogenic peptides, combined with engineered chemical reactivities, form an appealing biomolecular system for potential nanobiotechnological applications [7,8]. A special advantage of amyloid peptides is that variants suitable for a particular application may be generated by chemical [9] or biotechnological methods [5]. Once the fibrils are formed, they possess high stability under physical and chemical conditions far from the physiological. The global disorder in amyloid fibrillar arrangement, however, usually stands in the way of their widespread usability in nanotechnology applications. Previously we have shown that amyloid β25–35 (Aβ25–35), a toxic fragment of Alzheimer's beta peptide, forms trigonally oriented fibrils on mica [10]. We have demonstrated that the oriented binding depends on an apparently cooperative interaction of a positively-charged moiety on the Aβ25–35 peptide with the K^+-binding pocket of the mica lattice, lending a high K^+-sensitivity for peptide binding and fibril assembly. Fibril binding to mica was essentially insensitive to other ions such as Na^+ [10,11]. The formation of oriented fibrils is the result of epitaxial polymerization. Such a fibril network may be used in nanotechnology applications, provided that a specific chemical labeling of the fibrils is available. We have recently shown that the mutant Aβ25–35 peptide containing a Cys residue (Aβ25–35_N27C) also forms trigonally oriented fibrils on mica while displaying chemical reactivity in the fibril [11]. To utilize such chemically reactive fibrils for further nanotechnological applications, it is desired to tune the spatial features of the oriented network with simply controlled parameters.

In the present work we tested the effect of peptide and KCl concentrations on the assembly dynamics of Aβ25–35 peptides. We find that whereas fibril growth rate increases linearly with peptide concentration above the critical concentration of 3.92 μM, KCl is a competitive inhibitor of the assembly process. By adjusting the experimental variables within the optimal concentration ranges determined here, the structural details of the oriented Aβ25–35_N27C network may be finely tuned.

2. Materials and methods

2.1. Sample preparation

N27C mutant Aβ25–35 (^{25}GSCKGAIIGLM^{35}-amide) peptide (Aβ25–35_N27C) was produced by solid-state synthesis [9]. Sample preparation was carried out as documented previously [11]. Briefly, the lyophilized peptide was dissolved in DMSO (50.0 mg/ml) and diluted in 10 mM sodium phosphate buffer (10 mM Na_2HPO_4–NaH_2PO_4, pH 7.4, 0.02% NaN_3) supplemented with different concentrations of KCl as required by the specific experiments. To maintain a reductive environment and to prevent sulfhydryl oxidation and the formation of disulfide bridges between neighboring peptides, DTT was added to all buffer solutions at 20 mM concentration. Reducing environment was maintained throughout the experiments in order to avoid the influence of peptide dimerization on fibril growth kinetics. Insoluble aggregates were removed by high-speed centrifugation (Beckman Optima, 200,000 *g*, 30 min). Final concentration ranged between 0.5 and 2 mg/ml. Peptide concentration was measured with the quantitative bicinchoninic acid assay [12]. Aliquots of the sample were quick frozen in liquid nitrogen and stored at −80 °C for further use. After thawing the sample was diluted with buffer to the required concentrations (7.75–124 μM).

2.2. In situ atomic force microscopy

AFM measurements were carried out as described previously [10,11,13–16]. 100 μl samples were applied to freshly cleaved mica surface (V2 high-grade mica, #52-6, Ted Pella, Inc., Redding, CA). AFM scanning was started within 10 s after sample application. The samples were imaged with AFM in buffer under reducing conditions (20 mM DTT freshly added) to prevent disulfide-bridge formation. Non-contact mode AFM images were acquired with an Asylum Research MFP3D instrument (Santa Barbara, CA) using silicon-nitride cantilevers (Olympus BioLever, typical resonance frequency in buffer 9 kHz). Time-lapse AFM images of Aβ25–35 fibril growth on mica were recorded by repetitively scanning 2-μm-wide areas. 512 × 128-Pixel images were collected with no interleave pause at a typical scanning frequency of 1 Hz and at a high feedback set point. The time elapsed between consecutive images, hence the time resolution of the in situ AFM measurements, was 128 s. The approximately 10-second uncertainty related to the initiation of the time-lapse recording (setting of t_0) was less than 10% of the time resolution of the time-lapse recording.

2.3. Scanning force kymography

Scanning force kymography measurements were carried out as described previously [16]. Briefly, non-contact mode images of epitaxially growing amyloid fibrils were first acquired in order to establish the fibril growth directions. Scan angle was adjusted so that the fast (horizontal) scan direction was parallel with the chosen fibril orientation (one of the three main orientations). Slow scan along the direction perpendicular to the fibril axis was disabled, and consecutive linescans were assembled into a distance versus time image (kymogram). Images were typically acquired at 1–3 Hz scanning rate.

2.4. Image processing and data analysis

AFM images were analyzed by using algorithms built into the MFP3D driving software. Fibril growth rates were measured by obtaining the fibril length as a function of time in consecutive time-lapse images. Fibril length was measured as the full width at half maximum (FWHM) on topographical profile plots obtained along the fibril axis. For data analysis, we used IgorPro (Wavementrics, Lake Oswego, OR) and KaleidaGraph (v.4.0.2, Synergy Software).

3. Results

3.1. Oriented growth of Aβ25–35_N27C fibrils on mica

The formation of Aβ25–35_N27C fibrils on mica was investigated in time-dependent experiments. Time-lapse AFM experiments showed that seeds appear on the mica surface from which fibrils grow in one of the three main orientational directions (see Figs. 1, 2 and 4). Fibril growth proceeded until the fibril end reached a roadblock, typically in the form of another fibril lying across its path of growth. Once a growing fibril hit the side of an already developed fibril, its growth stopped (see Figs. 1, 2 and 4). Depending on the peptide and KCl concentrations, the formation of the oriented network took place on a time scale of a few minutes to hours. The global appearance of the oriented fibril network was similar in the case of the wild type and mutant peptides (Fig. 1a and b). There was an angle of 60° between fibril orientation directions, similarly to earlier observations [11]. There were differences in the growth dynamics of the wild-type and mutant fibrils, however. We observed that at identical ionic conditions and initial peptide concentrations wild-type fibrils grew faster (0.105 nm/s ± 0.014 nm/s SEM) than the mutant (0.046 nm/s ± 0.005 nm/s SEM). We also observed that the mutant fibrils were significantly thicker (mean topographical height: 3.01 nm ± 0.04 nm SEM) than the wild-type (mean topographical height: 2.74 nm ± 0.05 nm SEM) (Student's t probability < 0.0001),

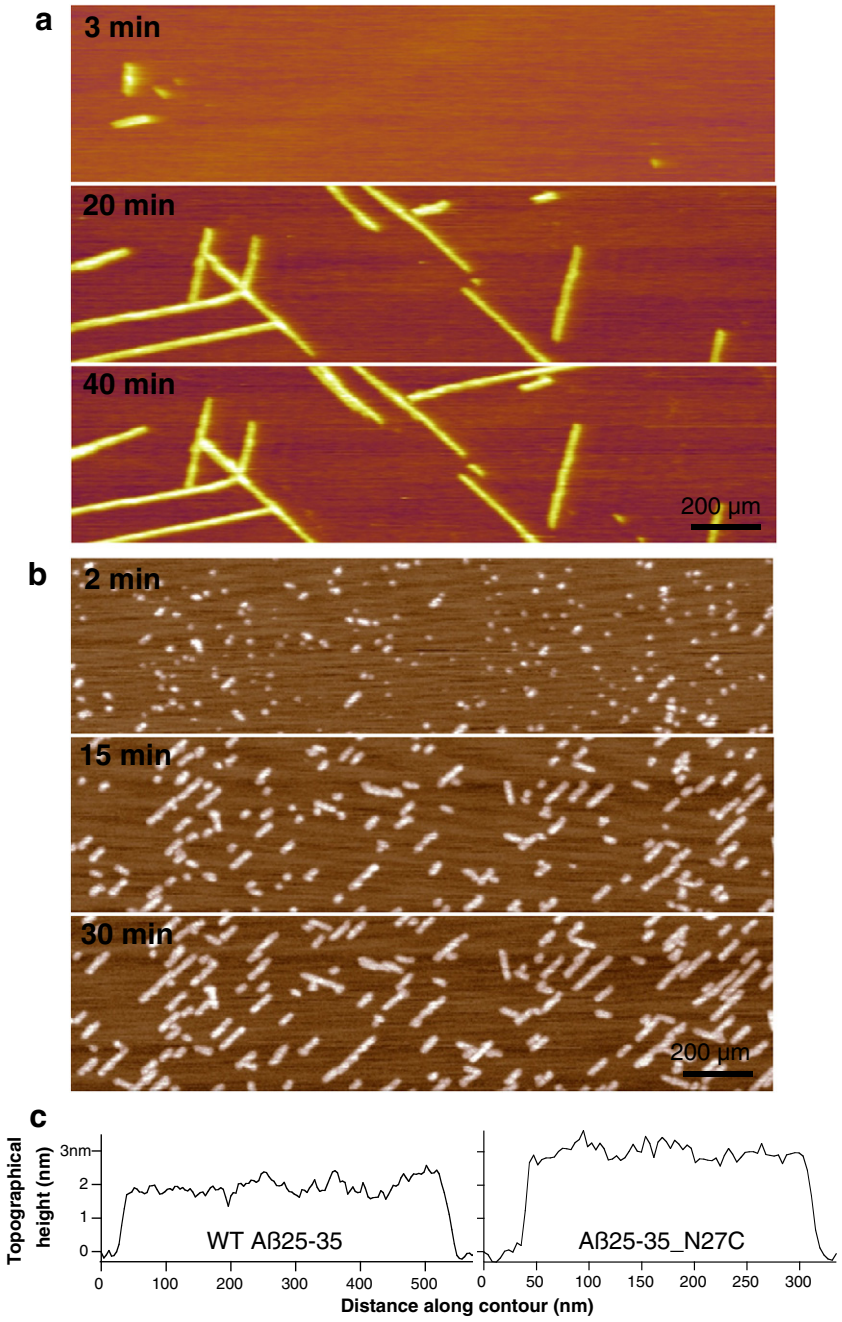

Fig. 1. Comparison of the wild-type and mutant Aβ25–35 fibrils. a. In situ AFM recording of the epitaxial assembly of wild-type Aβ25–35 fibrils on mica. b. In situ AFM recording of the epitaxial assembly of the mutant Aβ25–35_N27C fibrils on mica. c. Axial topographical profile of wild-type (left) and mutant (right) Aβ25–35 fibrils.

but their surface roughness, measured as the standard deviation of topographical height, was similar (~10% of mean height) (Fig. 1c).

3.2. Effects of peptide concentration on the kinetics of Aβ25–35_N27C fibril assembly

The effect of peptide concentration on the growth of Aβ25–35_N27C fibrils is shown in Figs. 2 and 3. Increasing the peptide concentration resulted in faster growth and denser fibrillar network (Fig. 2). As an example, at a peptide concentration of 15.5 μM (and at a KCl concentration of 2 mM) only few fibril seeds were observed and fibrils grew only few tens of nanometers in half an hour (Fig. 2a). By contrast, increasing the peptide concentration fourfold to 62 μM resulted in a very dense network (Fig. 2b). Fibrils grew to termination within 5 min. In Fig. 2b, top image, a gradient of fibril density and length can be observed, which is related to temporal evolution of the network along the top-down scanning direction. After 6 min no significant further changes in the global structure of the oriented fibrillar network could be observed (Fig. 2b, middle and bottom). The average fibril growth rate measured as a function of peptide concentration (at 1 mM KCl concentration) is shown in Fig. 3. Fibril growth rate varied linearly as a function of peptide concentration across the investigated concentration range. Below a critical concentration no fibril growth could be observed. The critical concentration, calculated as the x-intercept of the linear fit to the fibril growth rate versus peptide concentration data, is 3.92 μM.

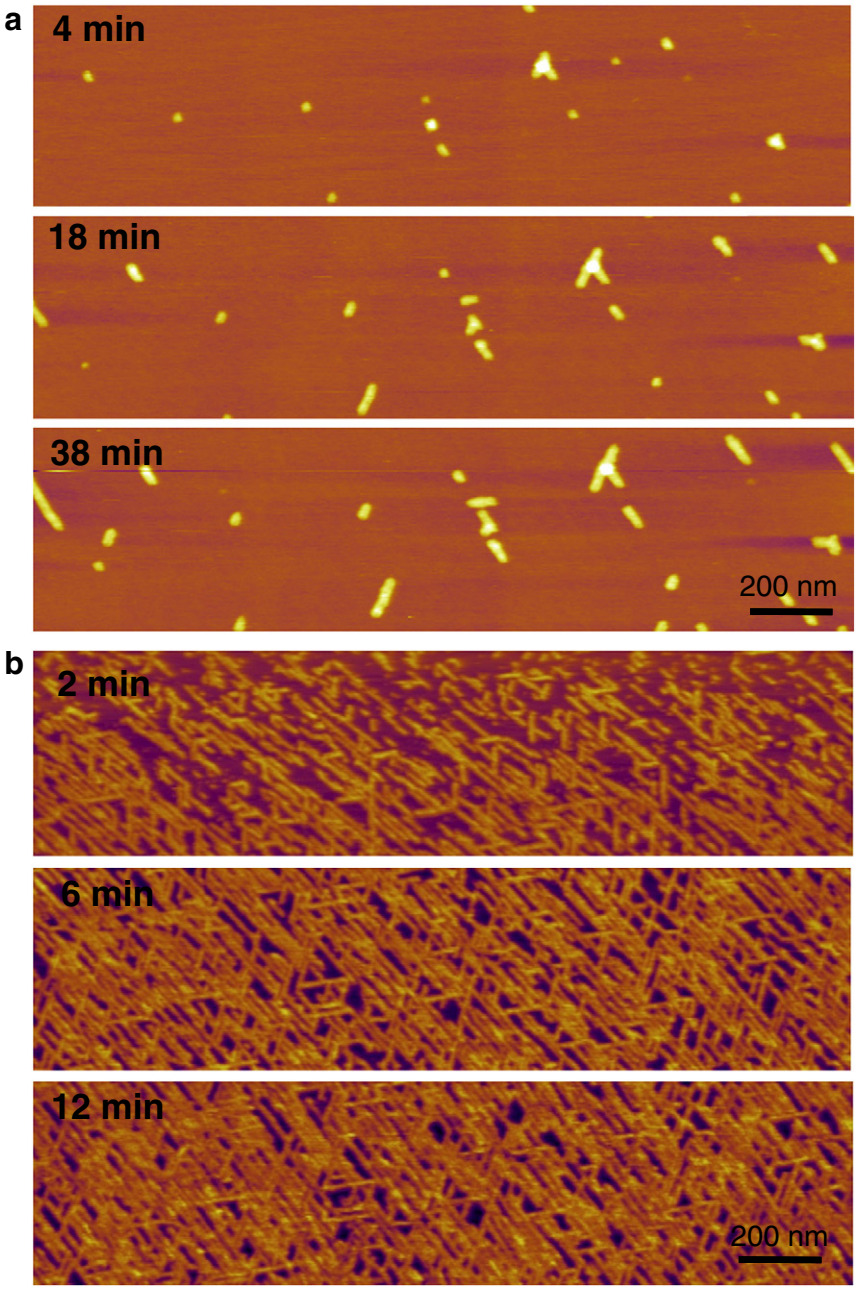

Fig. 2. Epitaxial assembly of Aβ25–35_N27C fibrils on mica as a function of peptide concentration. a. Time-resolved AFM images of growing Aβ25–35_N27C fibrils at a peptide concentration of 15.5 μM. b. Time-resolved AFM images of growing Aβ25–35_N27C fibrils at a peptide concentration of 62 μM. KCl concentration was 2 mM in both experiments.

3.3. Effect of KCl concentration on the kinetics of Aβ25–35_N27C fibril assembly

The effect of KCl concentration on the growth of Aβ25–35_N27C fibrils is shown in Figs. 4 and 5. KCl had an overall inhibitory effect on fibril assembly. At a peptide concentration of 62 μM doubling the KCl concentration from 8 mM to 16 mM resulted in a nearly complete inhibition of seed formation and fibril growth (Fig. 4b). A few fibrils grew only a few tens of nanometers on a time scale of more than an hour. To investigate the combined effect of KCl and peptide concentrations, the growth rate of Aβ25–35_N27C fibrils was measured at increasing KCl concentrations at each investigated peptide concentration. Fig. 5 shows the fibril growth rates in the investigated parameter space. Fibril growth rate varied across two orders of magnitude (~0.006–0.4 nm/s). At high peptide concentrations (124 μM) fibril growth could be discerned only in the presence of high KCl concentration (16 mM), otherwise the fibrils assembled on a time scale much faster than the AFM scan rate. At low peptide concentrations even moderate concentrations of KCl resulted in a nearly complete inhibition of fibril growth. Although KCl inhibited fibril assembly, in the concentration range of 1–4 mM we sometimes observed an enhancement of fibril assembly rate (Fig. 5, asterisks). In this KCl concentration range the rate of fibril assembly displayed a local maximum.

3.4. Scanning force kymography of Aβ25–35_N27C fibrils

In the fibril length versus time plots of Aβ25–35_N27C fibrils a stop-and-go feature could be discerned (Fig. 6a, arrows). Apparently the growth of the fibrils occasionally comes to a halt. To explore the dynamics of assembly and disassembly of individual Aβ25–35_N27C fibrils

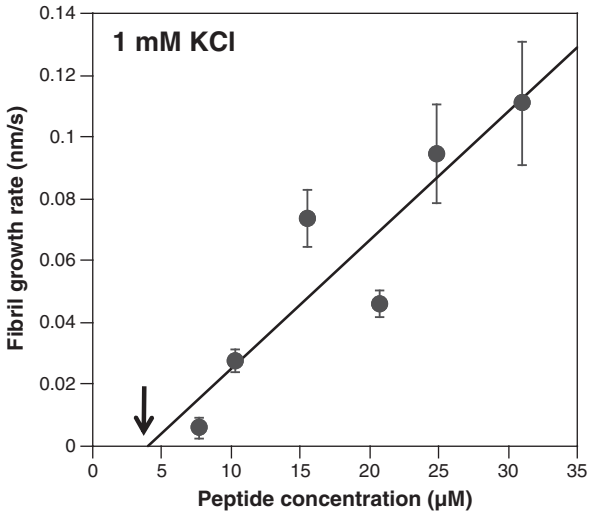

Fig. 3. Aβ25–35_N27C fibril growth rate as a function of peptide concentration. x-Intercept of linear fit (arrow, 3.92 μM) indicates critical peptide concentration of amyloid fibril assembly. The graph shows data for experiments at 1 mM KCl concentration.

with a higher temporal resolution, scanning force kymographic measurements were carried out. Fig. 6b shows a scanning force kymogram, in which three independent fibrils positioned along a common axis can be observed. The position of the ends of the fibrils can be followed as a function of time with large spatial (4 nm) and temporal resolution (1 s). Two of the three fibrils display increase in length, whereas the third one displays disassembly. Neither fibril growth, nor disassembly occurs continuously as a function of time. Rather, steps and pauses can be clearly observed.

4. Discussion

In the present work we investigated the epitaxially driven assembly dynamics of a mutant Aβ25–35 amyloid peptide, Aβ25–35_N27C. We have previously shown that Aβ25–35_N27C forms a trigonally oriented network on the surface of mica just like the wild-type peptide, and the binding is highly sensitive to KCl concentration [11]. By comparison, the binding of fibrils to mica was not inhibited by large concentrations of NaCl. The K^+-ion specificity of peptide binding likely stems from the structural features of the mica surface. Aβ25–35_N27C fibrils carry the special advantage of being chemically addressable, opening the possibilities of nanotechnological applications [11]. To efficiently control the structure of the oriented fibril network for nanotechnological and nanoelectronic applications, it is necessary to understand the role of experimental variables. Here we measured the effect of the two main determinants of the kinetics of epitaxial assembly: peptide concentration and KCl concentration.

We observed that both the wild-type and mutant fibrils assembled into globally similar oriented networks (Fig. 1a and b) but with different growth dynamics. Mutant fibrils grew significantly slower under identical solution conditions than the wild-type fibrils. Considering that the formation of disulfide bridges between the Cys27 side chains of neighboring peptides within the fibril may in principle accelerate fibril growth, our results indicate that the highly reductive conditions (presence of 20 mM DTT) efficiently prevented disulfide bridge formation. Therefore, a reducing environment was maintained throughout the measurements to alleviate the effect of peptide dimerization. The lower growth rate of mutant fibrils is probably related to the greater K^+-ion sensitivity observed before [11], and is likely due to the modified side-chain structure and properties. Interestingly, mutant fibrils had a greater diameter than the wild type (Fig. 1c). Considering that the Cys27 side chain in the mutant peptide is smaller in dimensions than the Gln27 side chain of the wild type, we speculate that larger diameter of the mutant fibril is caused by a greater number of component β-sheets.

Above a critical concentration the rate of fibril growth varied linearly with peptide concentration across the concentration range (7.75–124 μM) investigated. The critical peptide concentration, which is necessary to evoke the seeding and subsequent growth of the fibrils, was 3.92 μM. Previously, critical concentration values of 50 μM [17] and 100 μM [18] were measured for the assembly of Aβ1–40 fibrils in solution. The low critical concentration observed here is most likely caused by a catalytic effect of the surface [19,20]. For the oriented growth of the wild-type Aβ25–35 peptide we have previously measured a critical concentration of 10 μM in scanning force kymographic experiments [16]. In scanning force kymographic experiments, however, only the growing phase of fibrillogenesis was considered and the paused state of the fibrils was excluded from the analysis, thus yielding a slightly greater value for the critical concentration. Altogether the mica surface efficiently catalyzes the seeding and growth of Aβ25–35_N27C fibrils. At high peptide concentrations fibril growth rates up to 0.4 nm/s were measured. Considering the dimensions of a β-chain (4.7 Å, [4]), this growth rate is equivalent to the addition of one Aβ25–35_N27C molecule to the end of a pre-existing fibril every second. Because of the relatively low time-resolution of the time-lapse AFM method (minute time scale), faster fibril growth rates are difficult to measure at present. Furthermore, because of the steric constraints imposed on fibril growth by the trigonal arrangement, at high peptide concentrations the mica surface becomes rapidly saturated with fully-grown fibrils (Fig. 2b). Should such a constraint be absent, for example in unidirectional growth, it is probable that even greater fibril growth rates could be reached and measured.

Aβ25–35_N27C fibril assembly was inhibited strongly by the presence of small concentrations of KCl. Upon increasing KCl concentration the number of fibril seeds decreased and the growth of the fibrils became slower. Above 20 mM KCl the mica surface was completely devoid of fibrils. KCl is thus an efficient competitor of the binding of Aβ25–35_N27C peptides to mica because of the structural specificities of the substrate surface [21]. Fibril growth involves an initial, cation-sensitive step of peptide binding to mica coordinated primarily by the interaction between mica's K^+-binding pocket and the ε-amino group of Lys28 [14]. During the initial binding Aβ25–35_N27C molecules compete with K^+-ions for the binding sites on the mica surface lattice. Further binding of peptides to the initial fibril seed involves not only a direct interaction between mica and the peptide, but a hydrogen bonding between neighboring peptides as well. Because either set of bonds stabilizes the other type of interactions, the mica-driven oriented Aβ25–35_N27C fibril growth proceeds with an apparent cooperativity faster than either the binding of peptides on the mica surface or the aggregation of fibrils in solution. However, because the stabilization of the fibril involves further interaction of the newly-bound peptide and the K^+-binding pocket of mica, fibril growth is competitively inhibited by K^+ ions present in the solution. Our previous experiments have demonstrated that binding is specifically affected by K^+ ions, as NaCl at concentrations up to half molar did not have a significant effect on the oriented fibril network [10,11]. The parameter space for fibril growth (Fig. 5) suggests that the optimal KCl concentration for growing Aβ25–35_N27C fibrils on the mica surface is between 1 and 8 mM. Although K^+-ions act as competitive inhibitors of fibril growth, at low KCl concentrations fibril growth rate is sometimes enhanced (Fig. 5, asterisks). We speculate that the presence of a small concentration of K^+ ions slightly shifts the binding equilibrium between pre-existing fibrils and peptides so that it becomes more dynamic and kinetic traps are avoided. Conceivably, the competition between K^+ ions and the free peptide molecules enhances the fluctuation between the blocked and growing states of the fibril [16], which manifests in the stop-and-go feature of individual fibril assembly in scanning force kymographic

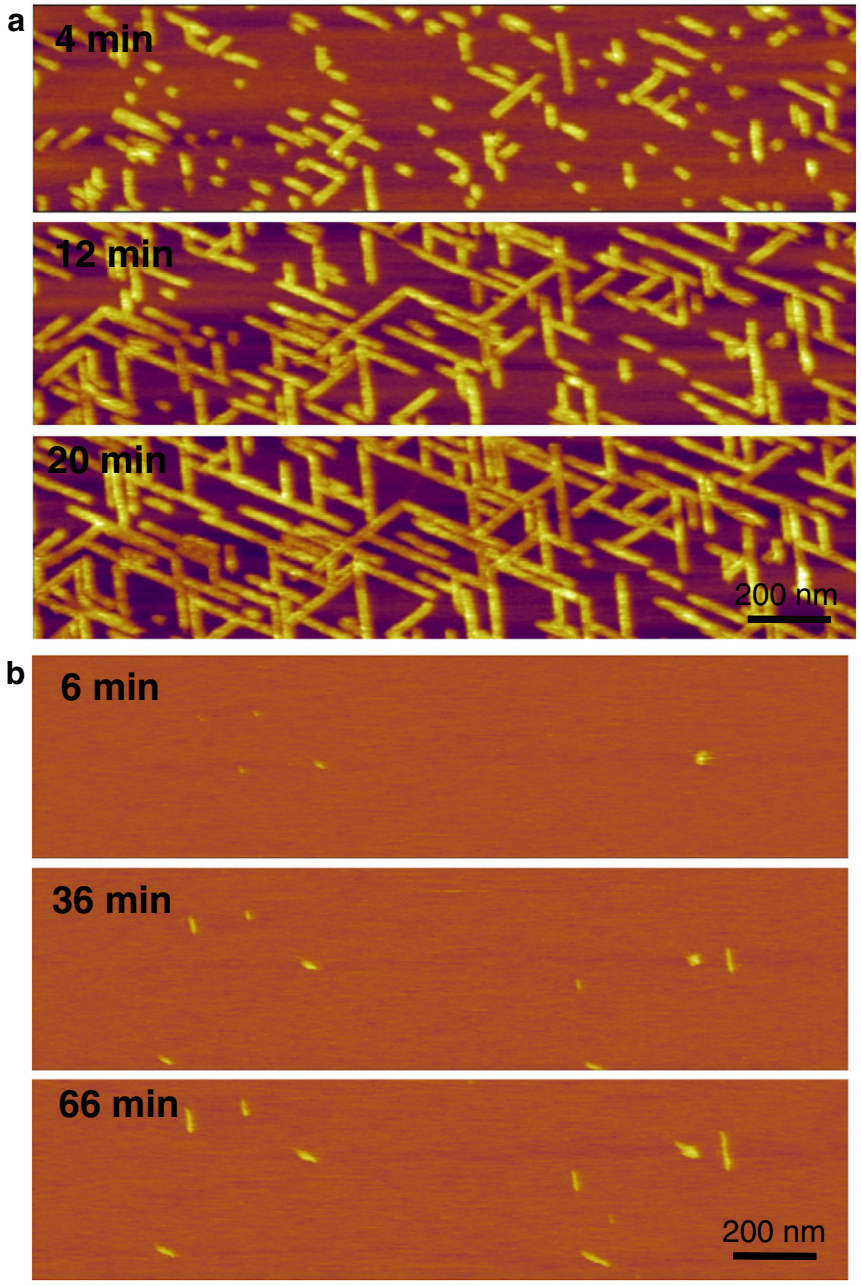

Fig. 4. Epitaxial assembly of Aβ25–35_N27C fibrils on mica as a function of KCl concentration. a. Time-resolved AFM images of growing Aβ25–35_N27C fibrils at a KCl concentration of 8 mM. b. Time-resolved AFM images of growing Aβ25–35_N27C fibrils at a KCl concentration of 16 mM. Peptide concentration was 62 μM in both experiments.

experiments (Fig. 6b). Further, detailed kymographic experiments that quantify the ratio of life times of the paused and growing states of Aβ25–35_N27C fibrils as a function of KCl concentration may provide a test of this idea.

The oriented Aβ25–35_N27C fibril network has a strong application potential. Because the Cys27 side chains within the Aβ25–35_N27C amyloid fibril can be chemically functionalized, dedicated molecular systems may be attached to the fibril surface via bifunctional cross-linkers. Such molecular systems include, for example, motor proteins, enzymes, or even nanogold particles, thereby generating oriented nanomechanical devices, nanosensors or nanoelectrical circuits, respectively. By controlling the peptide and KCl concentrations the fibril growth rate, hence the overall network density may be adjusted. Furthermore, by sequentially stopping and initiating fibril growth and alternating the addition of mutant and wild-type peptides, periodically or locally labeled fibrils may be constructed. Further in-depth testing may pave the way for the use of the oriented Aβ25–35_N27C fibril network in advanced nanotechnological applications.

5. Conclusions

In the present work we monitored the epitaxial assembly of the N27C mutant of Aβ25–35 fibrils, which form a trigonally oriented network on the surface of mica. The rate of fibril growth is enhanced by the free peptide concentration. The critical peptide concentration, below which fibril growth does not occur, is 3.92 μM. The low critical concentration indicates that mica is an efficient catalyzer of Aβ25–

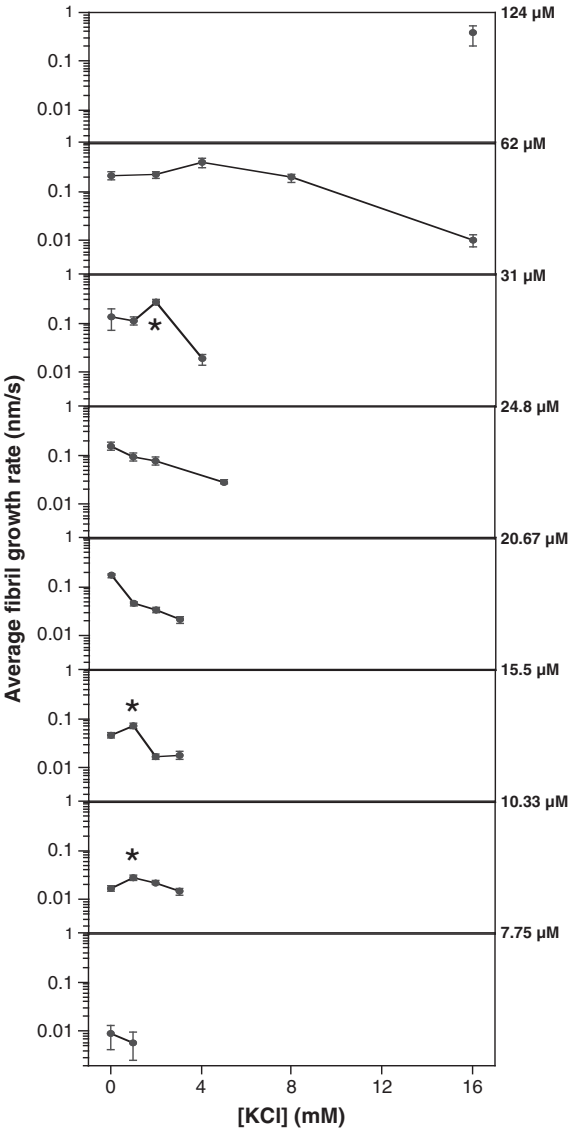

Fig. 5. Growth rate of Aβ25–35_N27C fibrils in the parameter space of peptide and KCl concentrations. Asterisks indicate significant increase in fibril growth rate at increasing KCl concentration.

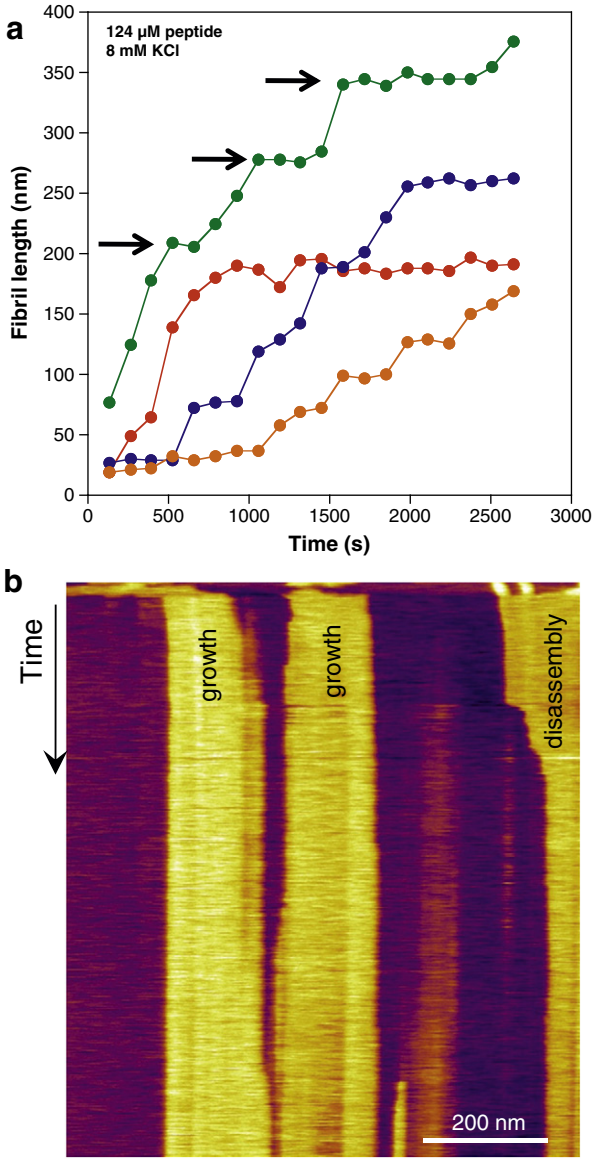

Fig. 6. Dynamics of epitaxial assembly and disassembly of Aβ25–35_N27C fibrils. a. Length of individual fibrils as a function of time. Arrows point at transiently paused states. b. Scanning force kymography of epitaxially growing Aβ25–35_N27C fibrils. The entire time span is 8 min.

35_N27C fibril assembly. K^+ ions strongly inhibit fibril growth, but at low K^+ concentration an activation effect is sometimes observed, which is probably due to the enhanced dynamics of the peptide-fibril binding equilibrium. Altogether the optimal peptide and KCl concentrations for fibril assembly are 30–60 μM and 1–6 mM, respectively. By adjusting peptide and KCl concentrations within these concentration ranges, the details of the oriented fibril network can be finely adjusted. By specifically labeling the Cys27 side chain of Aβ25–35_N27C amyloid fibrils, regular arrays of biomolecular nanostructures such as nanomechanical devices (by attaching motor proteins), nanosensors (by using enzymes), or nanoelectrical circuits (by labeling with nanogold particles) may be constructed.

Acknowledgments

This work was supported by a grant from the Hungarian Science Foundation (OTKA K84133). The research leading to these results has received funding from the European Union's Seventh Framework Programme (FP7/2007–2013) under grant agreement no. HEALTH-F2-2011-278850 (INMiND).

References

[1] J. Hardy, D.J. Selkoe, The amyloid hypothesis of Alzheimer's disease: progress and problems on the road to therapeutics, Science 297 (2002) 353–3556.
[2] D.J. Selkoe, Alzheimer's disease: genes, proteins and therapy, Physiol. Rev. 81 (2001) 741–766.
[3] D.J. Selkoe, Folding proteins in fatal ways, Nature 426 (2003) 900–904.
[4] L.C. Serpell, Alzheimer's amyloid fibrils: structure and assembly, Biochim. Biophys. Acta 1502 (2000) 16–30.
[5] T. Scheibel, R. Parthasarathy, G. Sawicki, X.M. Lin, H. Jaeger, S.L. Lindquist, Conducting nanowires built by controlled self-assembly of amyloid fibers and selective metal deposition, Proc. Natl. Acad. Sci. U. S. A. 100 (2003) 4527–4532.
[6] M. Reches, E. Gazit, Casting metal nanowires within discrete self-assembled peptide nanotubes, Science 300 (2003) 625–627.
[7] E. Gazit, Use of biomolecular templates for the fabrication of metal nanowires, FEBS J. 274 (2006) 317–322.
[8] D. Hamada, I. Yanagihara, K. Tsumote, Engineering amyloidogenicity towards the development of nanofibrillar materials, Trends Biotechnol. 22 (2004) 93–97.
[9] M. Zarándi, K. Soós, L. Fülöp, Z. Bozsó, Z. Datki, G.K. Tóth, B. Penke, Synthesis of Aβ(1–42) and its derivatives with improved efficiency, J. Pept. Sci. 13 (2007) 94–99.

[10] Á. Karsai, L. Grama, Ü. Murvai, K. Soós, B. Penke, M.S.Z. Kellermayer, Potassium-dependent oriented growth of amyloid β25–35 fibrils on mica, Nanotechnology 18 (2007) 345102.
[11] A. Karsai, U. Murvai, K. Soos, B. Penke, M.S. Kellermayer, Oriented epitaxial growth of amyloid fibrils of the N27C mutant beta 25–35 peptide, Eur. Biophys. J. 37 (2008) 1133–1137.
[12] P.K. Smith, R.I. Krohn, G.T. Hermanson, A.K. Mallia, F.H. Gartner, M.D. Provenzano, E.K. Fujimoto, N.M. Goeke, B.J. Olson, D.C. Klenk, Measurement of protein using bicinchoninic acid, Anal. Biochem. 150 (1985) 76–85.
[13] Á. Karsai, Z. Mártonfalvi, A. Nagy, L. Grama, B. Penke, M.S.Z. Kellermayer, Mechanical manipulation of Alzheimer's amyloid β1–42 fibrils, J. Struct. Biol. 155 (2006) 316–326.
[14] Á. Karsai, A. Nagy, A. Kengyel, Z. Mártonfalvi, L. Grama, B. Penke, M.S.Z. Kellermayer, Effect of lysine-28 side chain acetylation on the nanomechanical behavior of Alzheimer amyloid β25–35 fibrils, J. Chem. Inf. Model. 45 (2005) 1641–1646.
[15] M.S. Kellermayer, L. Grama, A. Karsai, A. Nagy, A. Kahn, Z.L. Datki, B. Penke, Reversible mechanical unzipping of amyloid beta-fibrils, J. Biol. Chem. 280 (2005) 8464–8470.
[16] M.S. Kellermayer, A. Karsai, M. Benke, K. Soos, B. Penke, Stepwise dynamics of epitaxially growing single amyloid fibrils, Proc. Natl. Acad. Sci. U. S. A. 105 (2008) 141–144.
[17] L.O. Tjernberg, A. Pramanik, S. Björling, P. Thyberg, J. Thyberg, C. Nordstedt, K.D. Berndt, L. Terenius, R. Rigler, Amyloid β-peptide polymerization studied using fluorescence correlation spectroscopy, Chem. Biol. 6 (1999) 53–62.
[18] A. Lomakin, D.S. Chung, G.B. Benedek, D.A. Kirschner, D.B. Teplow, On the nucleation and growth of amyloid β-protein fibrils: detection of nuclei and quantitation of rate constants, Proc. Natl. Acad. Sci. U. S. A. 93 (1996) 1125–1129.
[19] T. Kowalewski, D.M. Holtzman, In situ atomic force microscopy study of Alzheimer's beta-amyloid peptide on different substrates: new insights into mechanism of beta-sheet formation, Proc. Natl. Acad. Sci. U. S. A. 96 (1999) 3688–3693.
[20] M. Zhu, P.O. Souillac, C. Ionescu-Zanetti, S.A. Carter, A.L. Fink, Surface-catalyzed amyloid fibril formation, J. Biol. Chem. 277 (2002) 50914–50922.
[21] M.F. Brigatti, S. Guggenheim, M. Poppi, Crystal chemistry of the 1 M mica polytype: the octahedral sheet, Am. Mineral. 88 (2003) 667–675.